AAS-22-023

VALIDATION OF LINEAR COVARIANCE ANALYSIS FOR NOVA-C CISLUNAR TRAJECTORY DESIGN

Quinn Moon*, Donald H. Kuettel †, David K. Geller‡, Sam Welsh §, Shaun Stewart ¶, Tim Crain ‖

Nova-C is a lunar lander designed by the private company Intuitive Machines to deliver small commercial payloads to the surface of the Moon. The first Nova-C lander is manifested on the IM-1 mission in early 2022. A nominal deterministic trajectory for the mission is being designed using NASA's Copernicus software. In this paper, linear covariance (LinCov) is used to assess orbit determination (OD) performance based on the nominal trajectory and a selected ground-station tracking schedule. An assessment of OD performance for key mission events including trajectory correction maneuvers (TCMs), lunar approach and lunar orbit insertion (LOI), and descent orbit insertion (DOI) are presented. LinCov analysis is also used to assess trajectory dispersion at each of these key mission events. Monte Carlo analysis is employed to validate these results. The long-term goal of this research is to develop and validate a fully integrated LinCov tool to simultaneously determine trajectory dispersion, OD performance, and maneuver delta-v dispersion.

INTRODUCTION

Key elements of the Nova-C mission are trajectory design and performance analysis. This includes an assessment of expected orbit determination (OD) performance and trajectory dispersion. The performance assessment is based upon expected initial trajectory dispersion and knowledge errors, maneuver execution errors, modeling errors, and expected OD errors given the ground-station tracking schedule and specifications. To achieve this, linear covariance (LinCov) analysis[1,2] is employed and validated with Monte Carlo analysis.[3,4] LinCov tools have been previously developed and validated for several missions, including: orbital rendezvous,[5] powered ascent,[6] earth atmospheric entry,[7] Mars atmospheric entry,[8] the Mars Pathfinder,[9] and lunar descent.[4] However, LinCov tools for cislunar trajectories from translunar injection to lunar orbit insertion have not been previously validated. The goal of this paper is to show that LinCov can be a viable tool for cislunar navigation and dispersion analysis.

*Graduate Student, Mechanical and Aerospace Engineering, Utah State University Space Dynamics Laboratory, 416E Innovation Avenue, North Logan, UT, 84341
†Aerospace Engineer, Flight Dynamics, Intuitive Machines, 3700 Bay Area Blvd #600, Houston, TX 77058
‡Professor, Mechanical and Aerospace Engineering, Utah State University Space Dynamics Laboratory, 416E Innovation Avenue, North Logan, UT, 84341
§Nova-C Ground Navigation Lead, Intuitive Machines, 3700 Bay Area Blvd #600, Houston, TX 77058
¶Nova-C Flight Dynamics/GN&C Lead, Intuitive Machines, 3700 Bay Area Blvd #600, Houston, TX 77058
‖Vice President, Intuitive Machines, 3700 Bay Area Blvd #600, Houston, TX 77058

M. Sandnas, D. B. Spencer (eds.), *Proceedings of the 44th Annual American Astronautical Society Guidance, Navigation, and Control Conference, 2022*, Advances in the Astronautical Sciences 179, https://doi.org/10.1007/978-3-031-51928-4_8

REFERENCE TRAJECTORY AND GROUND-STATION TRACKING SCHEDULE

The Nova-C reference trajectory and maneuvers in Earth-Centered Inertial (ECI) coordinates are shown in Figure 1. The nominal deterministic trajectory is generated by NASA's Copernicus software with midcourse correction maneuvers planned by Intuitive Machines. The ground-station tracking schedule is generated using visibility reports from four ground-stations.

The trajectory shown in Figure 1 begins as the Nova-C lander separates from SpaceX's launch vehicle, referred to as launch vehicle separation (LVS). The trajectory is then divided using midcourse corrections. These midcourse corrections consist of a larger commissioning maneuver (CM) and three smaller trajectory correction maneuvers (TCM's). The Nova-C lander is inserted into lunar orbit using a lunar orbit insertion maneuver (LOI). After performing several orbits, the Nova-C lander begins the descent orbit insertion maneuver (DOI) and descends to the lunar surface.

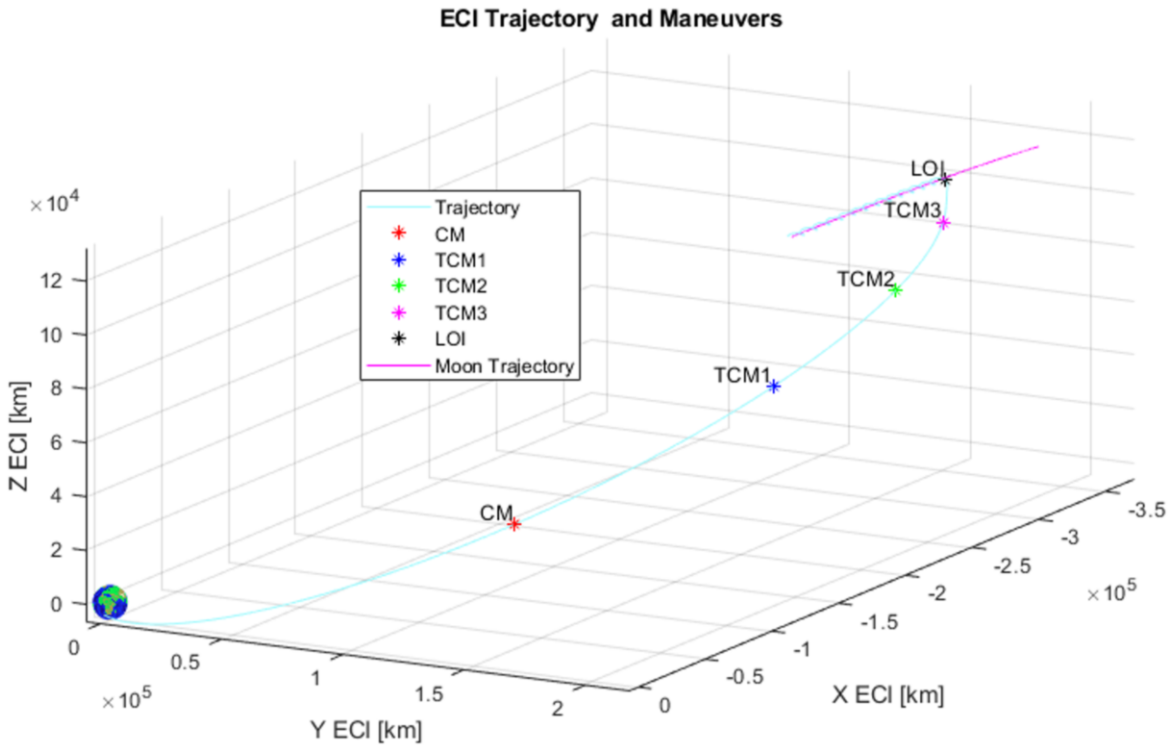

Figure 1: ECI Trajectory and Maneuvers

The maneuvers are further utilized to separate the trajectory into subsections, referred to as OD segments. Each OD segment is analyzed separately to determine OD performance and trajectory dispersion prior to each correction maneuver. To facilitate the Monte Carlo analysis in lunar orbit, the analysis for low lunar orbit (LLO) is further divided into individual orbits.

The contact schedule for ground-station tracking is shown in Figure 2. Four ground-stations are used for this study: Karnataka, India (D32); Morehead, Kentucky, United States (DSS17); Goonhilly, England (GHY6); Okinawa, Japan (OKN2). The contact schedule is planned such that Nova-C remains in contact with a single ground-station at any given time, except during lunar occultation.

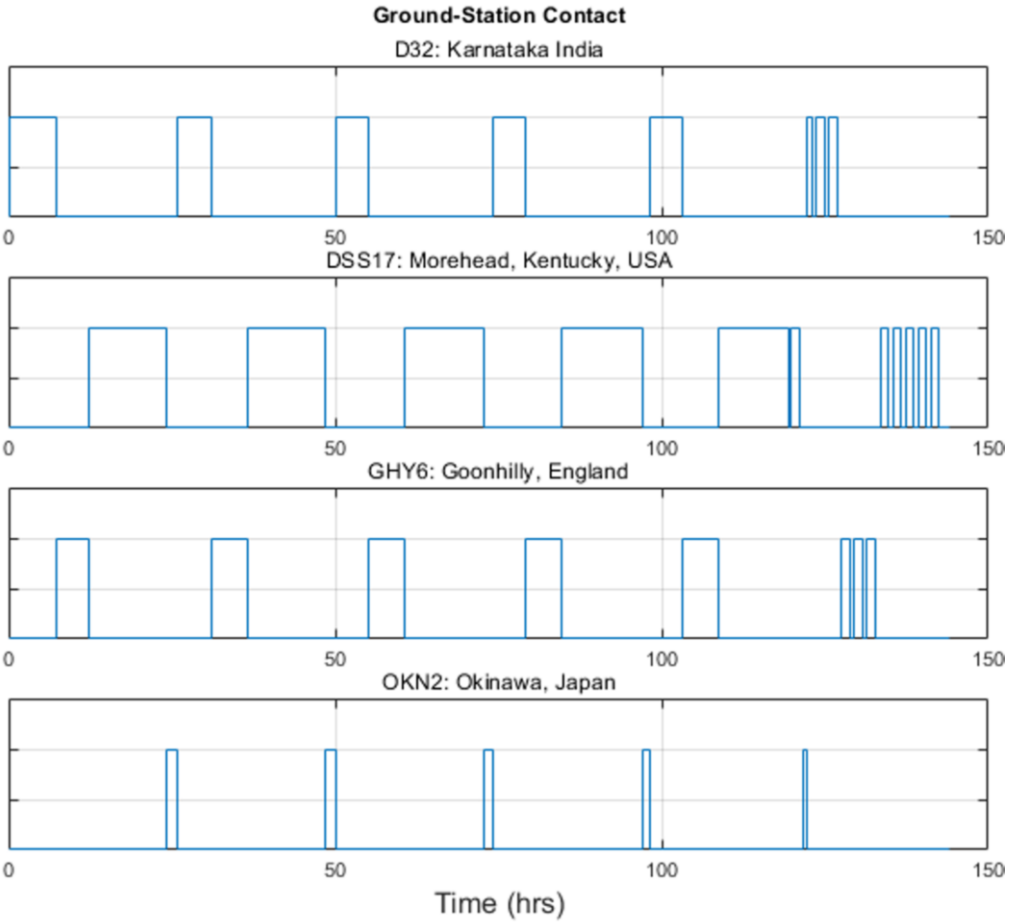

Figure 2: Ground-Station Contact Schedule

LINEAR COVARIANCE ANALYSIS

LinCov Equations

The LinCov state vector $\boldsymbol{x}$ consists of the Nova-C position and velocity vectors in J2000 inertial coordinates, solar radiation pressure (SRP) acceleration disturbances, and measurement biases

$$\boldsymbol{x} = \begin{bmatrix} \boldsymbol{r} \\ \boldsymbol{v} \\ \boldsymbol{\epsilon_{SRP}} \\ \boldsymbol{b_r} \\ \boldsymbol{b_{\dot{r}}} \end{bmatrix}$$

where the SRP acceleration and measurement biases are modeled as exponentially correlated random variables (ECRV's) with time-constants of approximately 10 days. The nonlinear dynamics can be written in the compact form

$$\dot{\boldsymbol{x}}(t) = f(\boldsymbol{x}(t), t) + \boldsymbol{w}$$

where $\boldsymbol{w}$ is the zero-mean Gaussian process noise. The system dynamics are linearized and discretized as follows

$$\boldsymbol{F} = \frac{\partial f}{\partial \boldsymbol{x}}$$
$$\boldsymbol{\Phi}(t_{k+1}, t_k) = e^{\boldsymbol{F}(t_{k+1} - t_k)}$$
$$\delta \boldsymbol{x}(t_{k+1}) = \boldsymbol{\Phi}(t_{k+1}, t_k)\delta \boldsymbol{x}(t_k) + \boldsymbol{\Upsilon}(t_k)\boldsymbol{w_{d,k}}$$

where $\boldsymbol{\Upsilon_k}$ represents the mapping for the discrete process noise $\boldsymbol{w_{d,k}}$. The linearized equations are then used to propagate the initial covariances. This paper studies both position and velocity dispersions and knowledge errors. Given the initial knowledge error covariance $\boldsymbol{P}$ and the initial dispersion covariance $\boldsymbol{C}$, the covariances are propagated as follows[10]

$$\boldsymbol{P}(t_{k+1}) = \boldsymbol{\Phi}(t_{k+1}, t_k)\boldsymbol{P}(t_k)\boldsymbol{\Phi^T}(t_{k+1}, t_k) + \boldsymbol{\Upsilon Q_{d,p}\Upsilon^T}$$
$$\boldsymbol{C}(t_{k+1}) = \boldsymbol{\Phi}(t_{k+1}, t_k)\boldsymbol{C}(t_k)\boldsymbol{\Phi^T}(t_{k+1}, t_k) + \boldsymbol{\Upsilon Q_{d,c}\Upsilon^T}$$

where $\boldsymbol{Q_{d,p}}$ and $\boldsymbol{Q_{d,c}}$ represent the covariance of the discrete process noise:

$$\boldsymbol{Q_{d,p}} = E[\boldsymbol{w_{d,p}}\boldsymbol{w_{d,p}^T}]$$
$$\boldsymbol{Q_{d,c}} = E[\boldsymbol{w_{d,c}}\boldsymbol{w_{d,c}^T}]$$

In addition to being propagated, the covariance of the knowledge errors is updated when measurements $z(t_k)$ are available at time t_k:

$$\boldsymbol{z}(t_k) = h(\boldsymbol{x}(t_k), t_k) + \boldsymbol{\nu}(t_k)$$

Linearizing the nonlinear measurement equation yields:

$$\boldsymbol{H} = \frac{\partial h}{\partial \boldsymbol{x}}$$

Using a sequential Kalman[10] filter, the covariance of the knowledge errors, $\boldsymbol{P}$, is updated using the equations below:

$$\boldsymbol{K}(t_k) = \boldsymbol{P}^{-}(t_k)\boldsymbol{H}^{\boldsymbol{T}}(t_k)\left[\boldsymbol{H}(t_k)\boldsymbol{P}^{-}(t_k)\boldsymbol{H}^{\boldsymbol{T}}(t_k) + \boldsymbol{R}\right]^{-1}$$
$$\boldsymbol{P}^{+}(t_k) = \left[\boldsymbol{I} - \boldsymbol{K}(t_k)\boldsymbol{H}(t_k)\right]\boldsymbol{P}^{-}(t_k)\left[\boldsymbol{I} - \boldsymbol{K}(t_k)\boldsymbol{H}(t_k)\right]^{T} + \boldsymbol{K}(t_k)\boldsymbol{R}\boldsymbol{K}(t_k)^{T}$$

The notations " $-$ " and " $+$ " denote before and after measurement incorporation occurs, respectively. The matrix $\boldsymbol{R}$ represents the strength of the measurement noise:

$$\boldsymbol{R} = E[\boldsymbol{\nu}(t_k)\boldsymbol{\nu}(t_k)^{T}]$$

MONTE CARLO ANALYSIS

A batch least squares estimator[11]within a Monte Carlo simulation[12] is used to validate the LinCov results. More specifically, this work uses the batch filter capabilities of Goddard Space Flight Center's General Mission Analysis Tool (GMAT). A diagram of the individual navigation simulations within the larger Monte Carlo simulation is shown in Figure 3. First, the nominal state of the spacecraft is perturbed by $\Delta\boldsymbol{x}$, which is pulled from an initial state error covariance, to get the "Truth" trajectory. Next, measurements are generated along the Truth trajectory. Then, with the spacecraft thinking it's on the reference trajectory, the batch filter processes the measurements to provide an estimated state ($\boldsymbol{x}_{B,IC}$) and associated covariance of the spacecraft at the beginning of the data arc. Next, the estimated state of the spacecraft is propagated to a desired epoch to get the corrected trajectory.

The navigation error ($\delta\boldsymbol{x}_P$) is calculated by differencing the corrected trajectory from the truth trajectory at the desired epoch. This process is repeated $\boldsymbol{N}$ times and the statistics of the navigation error of the spacecraft due to measurement noise is computed using the $\boldsymbol{N}$ samples of $\delta\boldsymbol{x}_P$. The trajectory dispersion ($\delta\boldsymbol{x}_C$) is calculated by differencing the truth trajectory from the nominal trajectory at the desired epoch. This process is repeated $\boldsymbol{N}$ times and the statistics of the trajectory dispersion due to initial state errors, maneuver execution errors, and SRP disturbances is computed using the $\boldsymbol{N}$ samples of $\delta\boldsymbol{x}_C$.

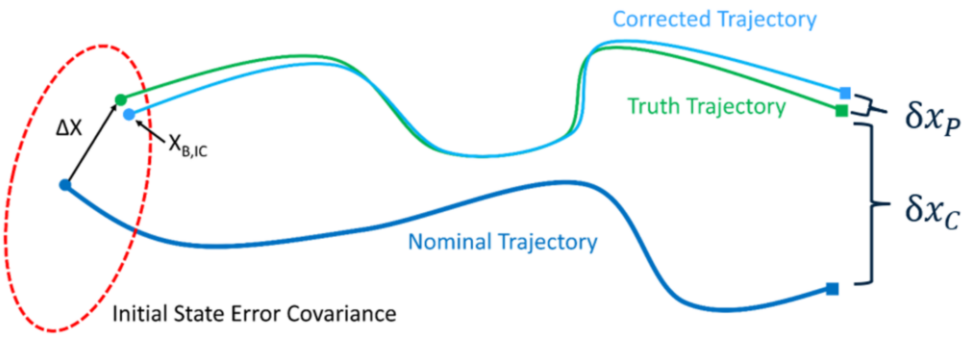

Figure 3: Monte Carlo Simulation

PROBLEM SETUP AND PARAMETERS

Initial Trajectory Dispersion and Knowledge Errors

At LVS, a conservative representation of the trajectory dispersion in terms of orbital elements is:

$$\begin{aligned}\sigma_{ra} &= 10 \text{ km} \\ \sigma_{rp} &= 5 \text{ km} \\ \sigma_i &= .1 \text{ degrees} \\ \sigma_\Omega &= .1 \text{ degrees} \\ \sigma_\omega &= .1 \text{ degrees}\end{aligned}$$

A conservative estimate of the initial knowledge errors is used:

$$\begin{aligned}\text{Position error: } \sigma_r &= 10 \text{ km / axis} \\ \text{Velocity error: } \sigma_v &= 1 \text{ m/s / axis}\end{aligned}$$

Ground-Station Measurement Specifications

The ground-stations provide two-way range-rate and two-way range measurements. Conservative estimates are used for the associated noise errors:

$$\begin{aligned}3\text{-}\sigma_{range} &= 10 \text{ m} \\ 3\text{-}\sigma_{range-rate} &= 1 \text{ cm/s}\end{aligned}$$

For the OD/navigation studies, a varying measurement duration is used to study the separate impacts of range-rate and range measurements. Furthermore, a measurement cutoff prior to maneuver execution is assumed. This cutoff accounts for the time needed for ground operations to process tracking data, compute required maneuvers, and uplink the maneuvers to the Nova-C lander.

Maneuver Execution Errors

The Nova-C mission is accomplished using closed-loop, inertial-hold maneuvers. The goal of each maneuver is to achieve a specified $\Delta \boldsymbol{v}$ in inertial space under closed-loop control with inertial measurement unit (IMU) feedback. This is accomplished via the IMU accelerometer and gyroscope measurements. However, accelerometer and gyroscope measurement errors produce inline and lateral maneuver execution errors. These maneuver execution errors are modeled mathematically and included in the dispersion studies.

The maneuver execution model is derived from the Nova-C lander's IMU data (see Appendix A). The Nova-C lander utilizes two IMU's for redundancy and the worse case IMU performance is assumed in the analysis. Using the IMU characteristics, a numerical analysis is performed by varying the maneuver size from 3 m/s to 1,000 m/s and by varying the spacecraft mass from 1,430 kg to 1,920 kg. The results of the IMU numerical analysis for the varying maneuver sizes and spacecraft masses are shown in Figure 4.

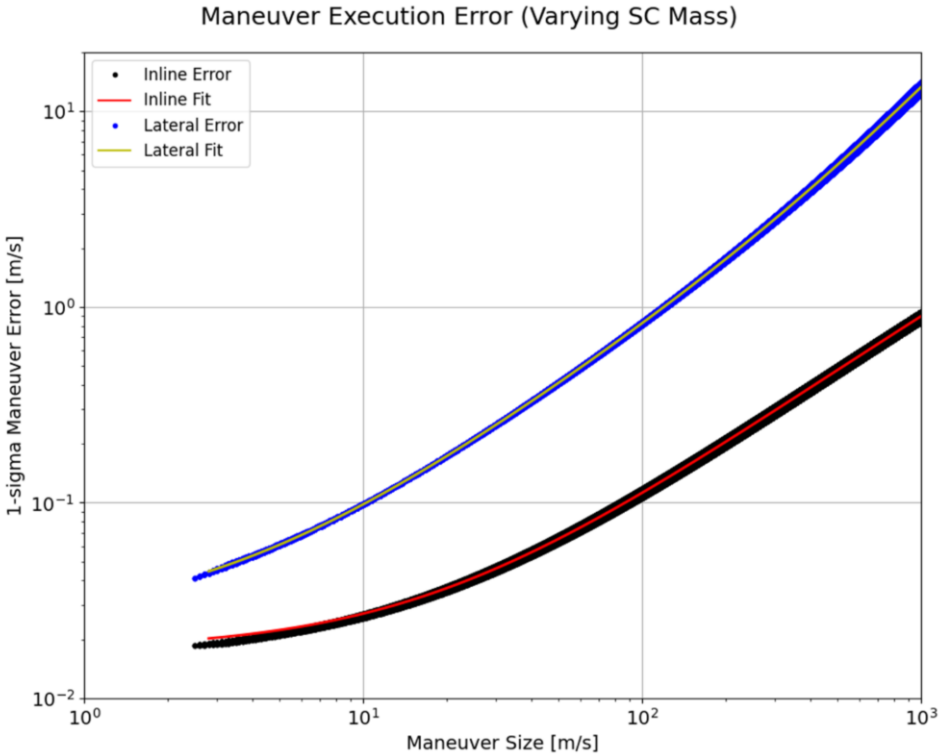

Figure 4: Polynomial fit of the inline and lateral 1-σ closed-loop maneuver execution error.

The inline (i) and lateral (l) maneuver error data is fitted using a least-squares polynomial fit giving the following equations for the 1-σ Δv error as a function of maneuver size:[13]

$$\sigma_i = 1.250 \times 10^{-11}||\Delta \boldsymbol{v}||^3 - 8.914 \times 10^{-8}||\Delta \boldsymbol{v}||^2 + 9.553 \times 10^{-4}||\Delta \boldsymbol{v}|| + 1.754 \times 10^{-2}$$
$$\sigma_l = -1.065 \times 10^{-9}||\Delta \boldsymbol{v}||^3 + 6.987 \times 10^{-6}||\Delta \boldsymbol{v}||^2 + 7.328 \times 10^{-3}||\Delta \boldsymbol{v}|| + 2.397 \times 10^{-2}$$

As Figure 4 shows, the cubic polynomials fit the maneuver execution data well regardless of spacecraft mass. This shows the validity of the polynomial fit throughout the entire Nova-C mission as the mass of the spacecraft changes. Finally, it is important to note that the maneuver execution data is unavailable below 3 m/s because this is the smallest maneuver that can be executed in a closed-loop fashion. For the purposes of the dispersion studies shown, a maneuver size of 3 m/s is used.

Environment Modeling Errors

Each OD segment includes gravitational effects from the Earth, Moon, and Sun. The LinCov analysis treats each body as a point mass, while the Monte Carlo utilizes a 8×8 gravity model for Earth and the Moon. This difference in modeling is negligible until LLO where the higher-order terms of the lunar gravity model become important.

This study also includes the effects of SRP acceleration disturbances. The following data is given to calculate the SRP acceleration acting on the Nova-C lander

$$\text{Surface Area to Mass Ratio: } \frac{A}{m} = .0035 \ \frac{m^2}{kg}$$
$$\text{Solar Flux: } S_f = 1359.39 \text{ W}$$
$$\text{Speed of Light: } c = 2.997 \times 10^8 \ \frac{m}{s}$$
$$\text{Acceleration due to SRP: } \frac{S_f}{c}\frac{A}{m}\rho$$

where ρ is the area-varying coefficient of reflectivity. The value of ρ ranges from 0 to 2 and accounts for both the spacecraft's coefficient of reflectivity and the spacecraft's attitude.

The LinCov analysis conservatively models the SRP acceleration as a constant random vector (in 3-dimensions) with a mean value of 1.587 $\times 10^{-8}$ m/s^2 (ρ = 1) and a standard deviation of 0.53 $\times 10^{-8}$ m/s^2 1-σ/axis (ρ = 0.33). The Monte Carlo analysis more realistically models the SRP acceleration as a constant random vector pointing opposite the Sun where ρ is sampled from a uniform distribution between 0 and 2.

LINCOV OD PERFORMANCE ANALYSIS AND VALIDATION

Case Study Setup

This section presents the results of the LinCov OD performance analysis for each OD segment and its validation with Monte Carlo analysis. The results are based on the nominal reference trajectory, ground-station tracking schedule, and ground-station measurement errors. Seven different OD segments are analyzed: five segments from LVS to LOI, and two LLO segments. The first five OD segments are LVS to CM, CM to TCM1, TCM1 to TCM2, TCM2 to TCM3, and TCM3 to LOI. Measurement cutoff occurs four hours prior to the end of each segment. The first LLO segment is simply the 8th lunar orbit consisting of approximately one hour of measurements and 50 minutes of propagation. The second LLO segment consists of the last three lunar orbits with approximately one hour of measurements and four hours of propagation.

The LinCov analysis and the OD/Monte Carlo analysis are conducted for two case studies: 1) full range-rate and range measurements for the duration of the OD segment up to measurement cutoff, 2) Full range-rate and only three hours of range measurements prior to measurement cutoff.

Case 1: Full range-rate and range measurements

Case 1 entails analyzing each OD segment by incorporating both range-rate and range measurements with their associated measurement noise (measurement biases are not included in this analysis). Each OD segment is analyzed using a 10s measurement cadence. Measurement cutoff occurs four hours prior to the end of each OD segment.

Figure 5 shows the time-history of the knowledge errors for OD segment 1 (LVS to CM) generated by the LinCov analysis. The first and second subplots show the 3-σ root sum squared (RSS) knowledge errors of position and velocity, respectively. The third and fourth subplots show the ground-station coverage and how each station provides range and range-rate measurements, respectively. The diagonal elements of the covariance matrix $\boldsymbol{P}$ are extracted at the final time of each OD segment and compared to the results of the OD Monte Carlo analysis.

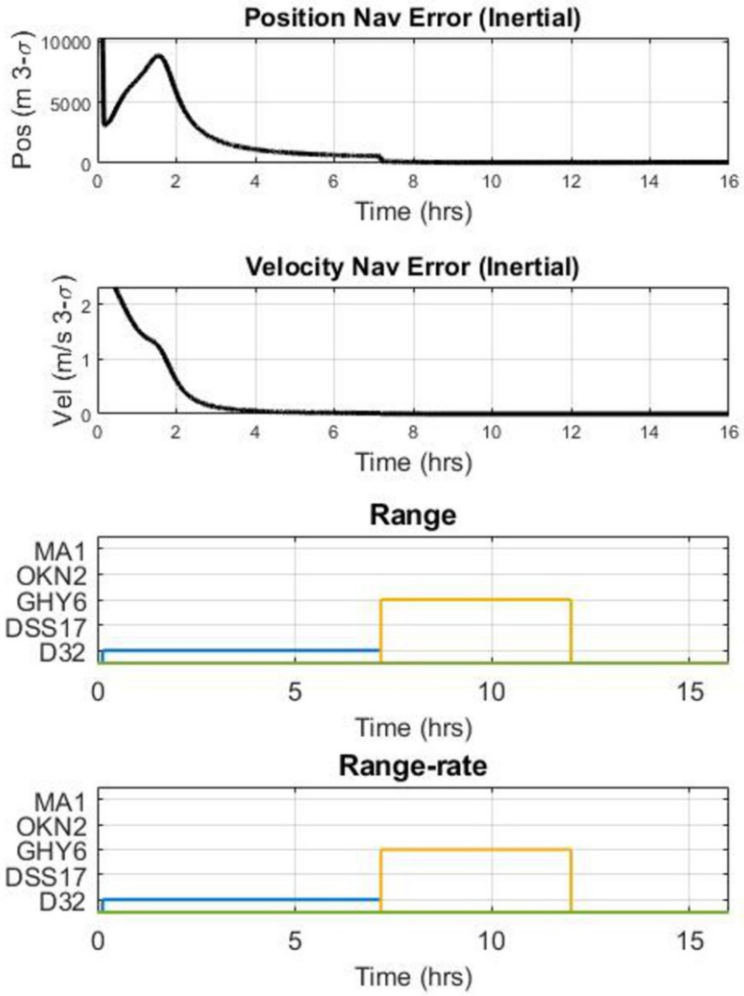

Figure 5: LVS-CM: Time-history of knowledge errors based on LinCov analysis

The inertial errors based on the LinCov analysis for each OD segment are reported in Table 1.

Table 1: Case 1: LinCov OD navigation results

OD Segment: -	**1** **LVS-CM**	**2** **CM-TCM1**	**3** **TCM1-2**	**4** **TCM2-3**	**5** **TCM3-LOI**	**6.1** **Orbit 8**	**6.2** **LLO-DOI**
Errors:							
3-σ r_x [m]	17.22	15.01	14.37	13.05	134.03	86.00	79.87
3-σ r_y [m]	23.33	18.17	19.26	26.05	51.76	128.53	192.28
3-σ r_z [m]	37.39	27.92	35.04	42.38	103.13	241.61	162.55
3-σ v_x [mm/s]	0.17	0.22	0.24	0.21	37.34	17.55	36.17
3-σ v_y [mm/s]	0.33	0.24	0.23	0.29	90.88	242.59	206.01
3-σ v_z [mm/s]	0.40	0.49	0.63	0.61	4.85	238.71	302.06

The LinCov results are then compared to the Monte Carlo results generated by GMAT software. The results for each OD segment based on the Monte Carlo analysis are shown in Table 2.

Table 2: Case 1: Monte Carlo OD navigation results

OD Segment: -	**1** **LVS-CM**	**2** **CM-TCM1**	**3** **TCM1-2**	**4** **TCM2-3**	**5** **TCM3-LOI**	**6.1** **Orbit 8**	**6.2** **LLO-DOI**
Errors:							
3-σ r_x [m]	17.13	15.01	14.38	13.00	134.89	89.72	94.59
3-σ r_y [m]	23.22	18.17	19.25	25.97	51.36	133.34	221.11
3-σ r_z [m]	38.46	27.92	35.14	42.44	103.66	242.68	187.57
3-σ v_x [mm/s]	0.17	0.22	0.24	0.21	37.26	14.21	29.96
3-σ v_y [mm/s]	0.33	0.24	0.23	0.29	91.79	244.98	230.73
3-σ v_z [mm/s]	0.42	0.49	0.64	0.61	4.84	243.88	323.63

An analysis comparing the LinCov and Monte Carlo results indicate that the greatest difference in the RSS knowledge errors, excluding the results for LLO to DOI, is 2.64%. The greatest difference in the RSS knowledge errors for LLO to DOI is 13.39%. This difference is attributed to the different gravity models and the four-hour propagation time prior to DOI.

Case 2: Full range-rate with three hours of range measurements

Figure 6 shows the time-history of the knowledge errors for OD segment 1 (LVS to CM) based on LinCov analysis. Note that unlike Case 1, the third subplot indicates that range measurements are only incorporated three hours prior to measurement cutoff.

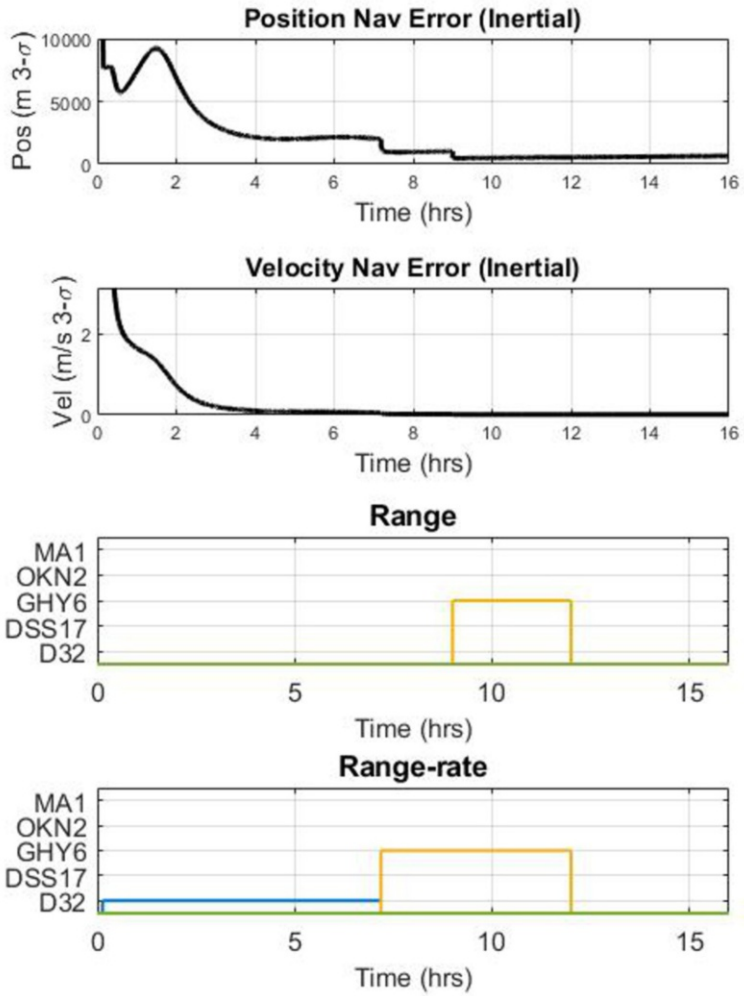

Figure 6: LVS-CM: Time-history of knowledge errors based on LinCov analysis with limited range measurements

The inertial errors based on the LinCov analysis for each OD segment are reported in Table 3.

Table 3: Case 2: LinCov OD navigation results

OD Segment:	**1**	**2**	**3**	**4**	**5**
-	**LVS-CM**	**CM-TCM1**	**TCM1-2**	**TCM2-3**	**TCM3-LOI**
Errors:					
3-σ r_x [m]	70.67	373.06	474.68	241.02	1,486.39
3-σ r_y [m]	97.49	160.37	322.32	282.37	259.27
3-σ r_z [m]	331.15	1,674.73	1,491.93	803.82	1,251.58
3-σ v_x [mm/s]	1.13	4.56	5.06	3.14	495.92
3-σ v_y [mm/s]	1.31	3.53	6.28	4.61	1,038.23
3-σ v_z [mm/s]	3.93	7.19	5.63	5.76	36.57

The LinCov results are then compared to the Monte Carlo results generated by GMAT software. The results for each OD segment based on the Monte Carlo analysis are shown in Table 4.

Table 4: Case 2: Monte Carlo OD navigation results

OD Segment:	1	2	3	4	5
-	**LVS-CM**	**CM-TCM1**	**TCM1-2**	**TCM2-3**	**TCM3-LOI**
Errors:					
3-σ r_x [m]	70.12	377.80	478.02	242.18	1,483.56
3-σ r_y [m]	97.29	160.32	322.97	280.99	258.29
3-σ r_z [m]	341.49	1,700.53	1,432.88	809.11	1,249.21
3-σ v_x [mm/s]	1.19	4.59	5.07	3.14	490.43
3-σ v_y [mm/s]	1.30	3.54	6.29	4.59	1,038.78
3-σ v_z [mm/s]	4.05	7.26	5.63	5.77	38.45

An analysis comparing the LinCov and Monte Carlo results indicate that the greatest difference in the RSS knowledge errors is 2.78%. Analysis and validation are not performed for LLO since the resulting range measurement duration would be too small to make an accurate comparison between the OD batch solutions and the sequential Kalman filter solutions.

Case 2 generated further interest in studying the impact of range measurement duration and ground-station location. Using LinCov analysis, Figures 7 and 8 show the 3-σ RSS knowledge errors plotted against 0-12 hours of range measurement duration. Tracking station GHY6 is in used for the first 4.5 hours, and then D32 is used for the remainder of this OD segment.

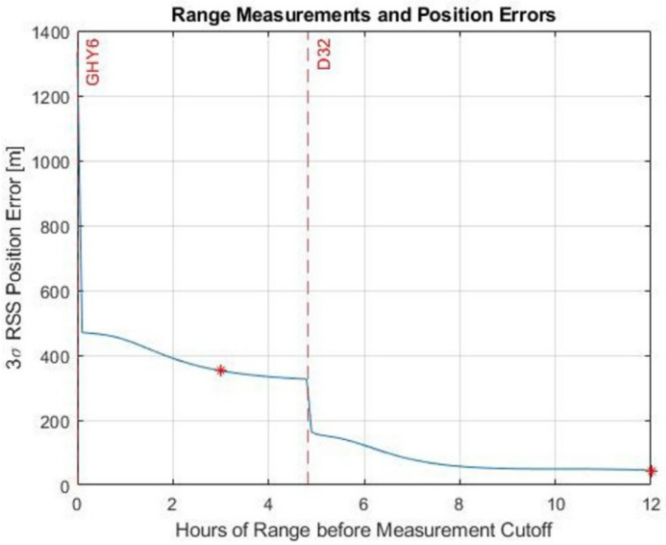

Figure 7: LVS-CM: RSS position knowledge errors as a function of range measurement duration

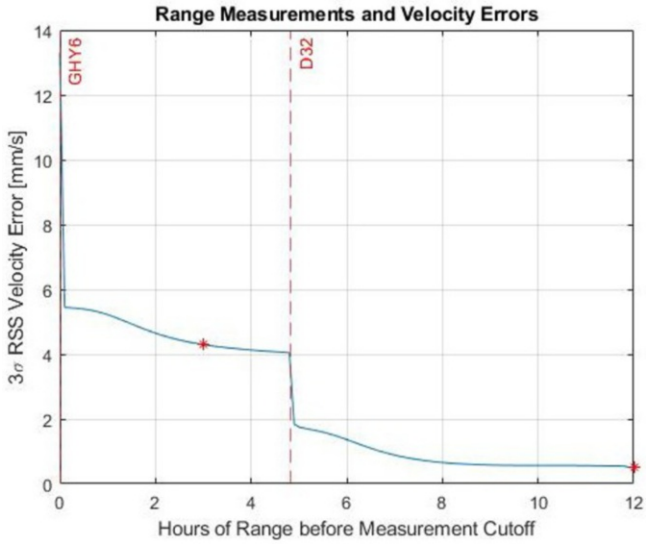

Figure 8: LVS-CM: RSS velocity knowledge errors as a function of range measurement duration

The red asterisks indicate the matching LinCov and Monte Carlo results from Cases 1 and 2. Assuming that all other data points on the plot would be validated by Monte Carlo, LinCov provides a fast tool that may be used to further study optimal range measurement duration.

LINCOV TRAJECTORY DISPERSION ANALYSIS AND VALIDATION

This section presents the results of the LinCov trajectory dispersion analysis and validation using Monte Carlo analysis. The error sources considered for the dispersion analysis are the initial state dispersion, maneuver execution errors, and SRP disturbances. The initial state dispersion implemented into the dispersion covariance matrix $\boldsymbol{C}$ are pulled from the final knowledge errors in the navigation study. The position and velocity dispersions are analyzed from each TCM to LOI due to the importance of being able to properly inject into lunar orbit in preparation for the final descent and landing. The total dispersion is expected to be the RSS of the individual dispersions due to initial state dispersions, maneuver execution errors, and the SRP disturbances.

The position and velocity dispersions at LOI based on LinCov analysis for TCM1 to LOI are presented in Table 5.

Table 5: Position and velocity dispersions at LOI based on LinCov analysis for TCM1-LOI

Error Source:	Initial State	Maneuver Execution	SRP Disturbances	Total
Errors:				
3-σ r_x [km]	0.337	49.401	1.142	49.416
3-σ r_y [km]	0.013	22.173	0.308	22.176
3-σ r_z [km]	0.289	32.752	0.874	32.765
3-σ v_x [m/s]	0.107	20.476	0.385	20.479
3-σ v_y [m/s]	0.239	32.405	0.786	32.416
3-σ v_z [m/s]	0.006	15.997	0.207	15.999

Position and velocity dispersions at LOI based on Monte Carlo analysis for TCM1 to LOI are presented in Table 6.

Table 6: Position and velocity dispersions at LOI based on Monte Carlo analysis for TCM1-LOI

Error Source:	Initial State	Maneuver Execution	SRP Disturbances	Total
Errors:				
3-σ r_x [km]	0.350	49.841	0.965	49.852
3-σ r_y [km]	0.015	22.778	0.173	22.790
3-σ r_z [km]	0.301	33.037	0.541	33.152
3-σ v_x [m/s]	0.112	20.832	0.260	21.015
3-σ v_y [m/s]	0.248	32.430	0.629	32.562
3-σ v_z [m/s]	0.005	16.484	0.217	16.085

An analysis comparing the LinCov and Monte Carlo results indicate that the greatest difference in the RSS dispersions for initial state and maneuver execution errors is 3.76%. The difference in the RSS dispersions for SRP is much larger, 35.81%. However, this larger difference is expected due to the different SRP models used in the LinCov and Monte Carlo analysis. Furthermore, the impact of SRP on the total dispersions is minimal.

The position and velocity dispersions at LOI based on LinCov analysis for TCM2 to LOI are presented in Table 7.

Table 7: Position and velocity dispersions at LOI based on LinCov analysis for TCM2-LOI

Error Source:	Initial State	Maneuver Execution	SRP Disturbances	Total
Errors:				
3-σ r_x [km]	0.281	29.330	0.442	29.334
3-σ r_y [km]	0.019	13.455	0.125	13.455
3-σ r_z [km]	0.247	21.133	0.342	21.137
3-σ v_x [m/s]	0.099	13.225	0.155	13.227
3-σ v_y [m/s]	0.200	19.540	0.305	19.547
3-σ v_z [m/s]	0.008	8.971	0.079	8.967

Position and velocity dispersions at LOI based on Monte Carlo analysis for TCM2 to LOI are presented in Table 8.

Table 8: Position and velocity dispersions at LOI based on Monte Carlo analysis for TCM2-LOI

Error Source:	Initial State	Maneuver Execution	SRP Disturbances	Total
Errors:				
3-σ r_x [km]	0.274	29.416	0.381	29.962
3-σ r_y [km]	0.019	13.198	0.066	13.803
3-σ r_z [km]	0.239	21.017	0.213	21.027
3-σ v_x [m/s]	0.097	13.069	0.103	13.425
3-σ v_y [m/s]	0.194	19.507	0.249	19.765
3-σ v_z [m/s]	0.007	8.817	0.084	9.199

An analysis comparing the LinCov and Monte Carlo results indicate that the greatest difference in the RSS dispersions for initial state and maneuver execution errors is 2.93%. The difference in the RSS dispersions for SRP is much larger, 29.58%. Again, this larger difference is expected due to the different SRP models used.

The position and velocity dispersions at LOI based on LinCov analysis for TCM3 to LOI are presented in Table 9.

Table 9: Position and velocity dispersions at LOI based on LinCov analysis for TCM3-LOI

Error Source:	Initial State	Maneuver Execution	SRP Disturbances	Total
Errors:				
3-σ r_x [km]	0.137	11.611	0.067	11.612
3-σ r_y [km]	0.025	5.791	0.023	5.791
3-σ r_z [km]	0.124	8.517	0.051	8.518
3-σ v_x [m/s]	0.057	5.720	0.026	5.721
3-σ v_y [m/s]	0.097	7.786	0.046	7.786
3-σ v_z [m/s]	0.006	3.609	0.013	3.609

Position and velocity dispersions at LOI based on Monte Carlo analysis for TCM3 to LOI are presented in Table 10.

Table 10: Position and velocity dispersions at LOI based on Monte Carlo analysis for TCM3-LOI

Error Source:	Initial State	Maneuver Execution	SRP Disturbances	Total
Errors:				
3-σ r_x [km]	0.136	11.486	0.056	11.510
3-σ r_y [km]	0.025	5.704	0.011	5.690
3-σ r_z [km]	0.123	8.656	0.029	8.397
3-σ v_x [m/s]	0.057	5.797	0.015	5.648
3-σ v_y [m/s]	0.097	7.707	0.036	7.678
3-σ v_z [m/s]	0.006	3.495	0.013	3.559

An analysis comparing the LinCov and Monte Carlo results indicate that the greatest difference in the RSS dispersions for initial state and maneuver execution errors is 3.75%. The difference in the RSS dispersions for SRP is much larger, 31.32%. Again, this larger difference is expected due to the different SRP models used.

Figure 9 shows the total trajectory dispersion in the B-Plane for each TCM to LOI. By analyzing the trajectory dispersion in the B-Plane, ground operations can better determine whether a maneuver is necessary. In Figure 9, the solid ellipses indicate the dispersions generated by LinCov and the dashed ellipses indicate the dispersions generated by the Monte Carlo analysis.

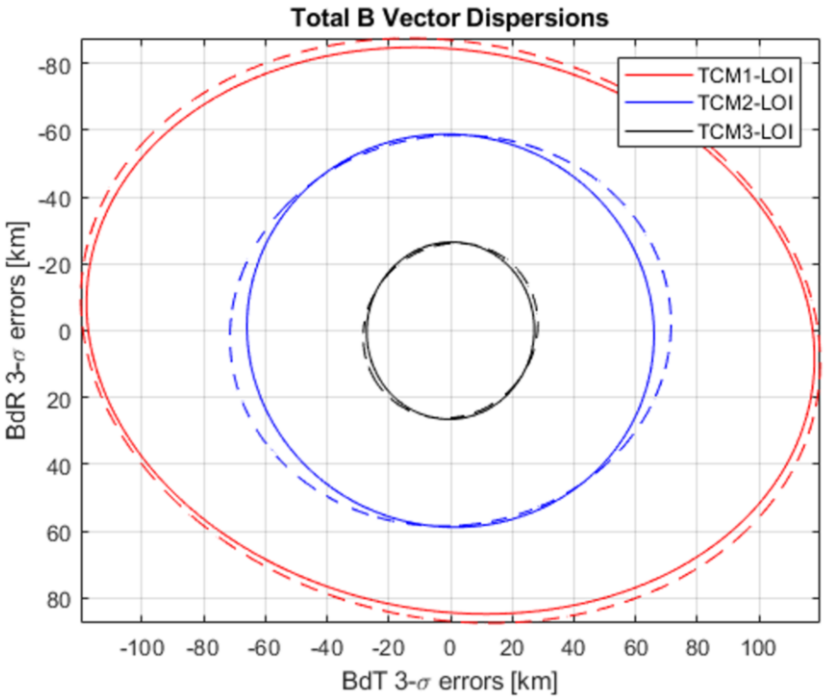

Figure 9: Total B-Vector Dispersions

CONCLUSION

The results of this paper provided a preliminary validation of linear covariance analysis for cislunar flight and lunar orbit using Monte Carlo analysis. Both OD/navigation performance and dispersion analysis were validated. The OD performance considered range-rate and range measurement noise and measurement duration. The dispersion analysis considered initial state errors, maneuver execution errors, and SRP disturbances. The LinCov results were validated using Monte Carlo analysis for the entire mission from launch vehicle separation to lunar orbit insertion to lunar descent orbit insertion.

APPENDIX

The maneuver execution error is divided into two parts: (1) errors from the accelerometers sensing the non-gravitational acceleration experienced by the spacecraft during the maneuver and (2) pointing errors during the execution of the maneuver from the gyroscopes. Both the accelerometer and gyroscope measurement errors are a result of errors due to the misalignment of the IMU axes, scale-factor uncertainties, random biases, and noise. Furthermore, the Nova-C mission uses two IMUs for redundancy HG1700[14] and SDI-500-A.[14] The mission needs to be accomplished with either IMU, so the worse case IMU specifications shown in Table 11 are used in the maneuver execution model.

Table 11: Nova-C IMU Characteristics

Parameter	**1σ Value**	**IMU**
Gyro Bias, b_g	7 deg/hr	HG1700
Gyro Scale Factor, S_g	260 ppm	HG1700
Gyro Angle Random Walk, η_g	0.17 deg/rt-hr	HG1700
Accel Bias, b_a	100 μg	SDI-500-A
Accel Scale Factor, S_a	520 ppm	HG1700
Accel Velocity Random Walk, η_a	58.3 μg/rt-hz	HG1700
Accel Misalignment, Γ_a	0.0333 deg	-
Initial Attitude Error, θ_0	0.333 deg	-

REFERENCES

[1] D. K. Geller, "Linear covariance techniques for orbital rendezvous analysis and autonomous onboard mission planning," *Journal of Guidance, Control, and Dynamics*, Vol. 29, No. 6, 2006, pp. 1404–1414.

[2] R. S. Christensen and D. Geller, "Linear covariance techniques for closed-loop guidance navigation and control system design and analysis," *Proceedings of the Institution of Mechanical Engineers, Part G: Journal of Aerospace Engineering*, Vol. 228, No. 1, 2014, pp. 44–65.

[3] D. Hennes and D. Izzo, "Interplanetary trajectory planning with Monte Carlo tree search," *Twenty-Fourth International Joint Conference on Artificial Intelligence*, 2015.

[4] K. DeMars and R. Bishop, "Navigation Analysis to Facilitate Precision Descent Navigation for Landing at the Moon," 01 2008.

[5] D. C. Woffinden and D. K. Geller, "Relative angles-only navigation and pose estimation for autonomous orbital rendezvous," *Journal of Guidance, Control, and Dynamics*, Vol. 30, No. 5, 2007, pp. 1455–1469.

[6] M. B. Rose and D. Geller, "Linear covariance techniques for powered ascent," *AIAA guidance, navigation, and control conference*, 2010, p. 8175.

[7] K. Jin, D. Geller, and J. Luo, "Development and validation of linear covariance analysis tool for atmospheric entry," *Journal of Spacecraft and Rockets*, Vol. 56, No. 3, 2019, pp. 854–864.

[8] T. Crain and R. Bishop, "Mars entry navigation: atmospheric interface through parachute deploy," *AIAA Atmospheric Flight Mechanics Conference and Exhibit*, 2002, p. 4501.

[9] R. M. Vaughan, P. H. Kallemeyn Jr, D. A. Spencer, and R. D. Braun, "Navigation flight operations for Mars Pathfinder," *Journal of spacecraft and rockets*, Vol. 36, No. 3, 1999, pp. 340–347.

[10] J. L. Crassidis and J. L. Junkins, *Optimal estimation of dynamic systems*, Vol. 2. Chapman & Hall/CRC Boca Raton, FL, 2004.

[11] S. Bae and B. Schutz, "ICESat/GLAS attitude determination using a batch least squares estimator during star tracker starless periods," *AIAA/AAS Astrodynamics Specialist Conference and Exhibit*, 2002, p. 4915.

[12] S. Raychaudhuri, "Introduction to monte carlo simulation," *2008 Winter simulation conference*, IEEE, 2008, pp. 91–100.

[13] D. Kuettel, "Closed-Loop Inertial-Hold Maneuver Execution Error Model," Intuitive Machine's Internal Documentation, December 2021.

[14] Honeywell, "HG1700 IMU Data Sheet," January 12, 2022.